Novel Measurement Procedure for Switched-Mode Power Supply Modal Impedances

Enrico Mazzola, *Student Member, IEEE*, Flavia Grassi, *Senior Member, IEEE*, and Alessandro Amaducci, *Member, IEEE*

***Abstract*—The measurement of modal impedances of switching-mode power supplies (SMPS) is of paramount importance in EMC applications, especially when designing EMI filters to suppress the conducted and radiated electromagnetic emissions is the target. A novel measurement technique which makes use of an impedance analyzer and a coupling transformer and allows extracting the complex value of common and differential mode noise-source impedance of a SMPS is proposed. The measurement procedure is first studied from the theoretical point of view, then experimentally validated with passive components, and eventually implemented in a CISPR-25 conducted emission test set-up to measure the magnitude and phase of modal impedances of an automotive SMPS under different operation conditions.**

***Index Terms*—Common Mode and Differential Mode, Conducted Emissions, Automotive Switched-Mode Power Supplies.**

I. Introduction

Switched-Mode Power Supplies (SMPS) are well known as one of the major contributor to electromagnetic interference (EMI). The topic is gaining more and more importance, especially in the automotive industry where, due to the electrification process of vehicles, the large use of SMPS poses new challenges in terms of conducted (CE) and radiated emissions (RE), which must be kept under control to fulfill the international standards on the one hand, and to protect sensitive electronics, such as the electronic central unit (ECU) and possible autonomous driving systems.

In order to achieve effective filtering of SMPS emissions, the knowledge of the input Common Mode (CM) and Differential Mode (DM) impedances in the frequency range of interest is of paramount importance. In the literature, only the magnitude is usually considered, and in practical applications it is quite common to talk about *high* or *low* source impedance only. However, with emerging technologies such as active EMI filtering techniques [1]–[4], information on the phase of the SMPS internal impedance is becoming of critical importance. Indeed, design methodologies not accounting for both magnitude and phase of SMPS modal impedances could even lead to EMI amplification as well as issues related to system instability.

International standards, such as CISPR 25 [5], describe the test setup to measure the emissions of automotive systems. To guarantee test repeatability, the device under test (DUT) shall be connected to a specific Line Impedance Stabilization Network (LISN), whose impedance, yet standardized, is quite far from the pure-resistive 50 Ω impedance [6] usually assumed for filter design.

Furthermore, measurement of the SMPS complex impedance is not a trivial task. In the literature, some methods have been recently proposed towards this goal. Among these, the Insertion Loss (IL) method in [7] foresees to measure the magnitude only, considering some simplifications. The phase is then retrieved by using the Hilbert transform. In the two probes approach proposed in [8], [9], the complex impedance is measured using an injection probe, a sensing probe, and a Vector Network Analyzer (VNA). In order to assure reliable impedance measurement, this method requires an accurate procedure of calibration, aimed at characterizing the frequency response of the involved probes as well as of parasitics effects in the whole frequency interval of interest. To overcome this limitation, the method in [10] was proposed, which still makes use of a VNA but involves a simplified procedure of calibration. This is achieved by introducing an *ad hoc* modified LISN, which may results to be either an advantage or a disadvantage of such a method depending on the specific application and context. More recently, an IL perturbation method was presented in [11], which resorts to the use of a filter with variable impedance and repeated measurement to extract the SMPS impedance in magnitude and phase. However, some of the assumptions involved in the theoretical derivation (e.g., the impedance of the LISN is assumed to be resistive and constant-valued in the whole frequency interval of interest) may non-neglibly impact on the accuracy of the obtained results in specific frequency intervals.

In this paper, a novel approach for the measurement of the complex CM and DM impedances of a SMPS under loading conditions is presented. The advantage of the proposed method lays in the simplicity in terms of involved test setup as well as of the procedure of extraction of the unknown impedances from measurement data. Namely, the method makes use of an Impedance Analyzer, which is specifically designed to perform impedance measurement over a wide frequency interval in a precise and repeatable way thanks to an Auto Balancing Bridge architecture [12]. The measurement instrument is then

This work has been supported by Schaffner Group, Switzerland. See https://www.schaffner.com/.

E. Mazzola is with the Automotive Department of Schaffner Group, Luterbach, Switzerland and with the Department of Electronics, Information and Bioengineering, Politecnico di Milano, Milan 20133, Italy (enrico.mazzola@schaffner.com).

F. Grassi is with the Department of Electronics, Information and Bioengineering, Politecnico di Milano, Milan 20133, Italy (flavia.grassi@polimi.it).

A. Amaducci is with the is with the Automotive Department of Schaffner Group, Luterbach, Switzerland (alessandro.amaducci@schaffner.com).

interfaced with the system under test through a suitably-designed hand-made transformer, whose parameters over frequency can be directly measured at the output ports. Such a coupling device is more versatile, since it can be hand-manufactured and customized to the specific characteristics of the SMPS under test, e.g., maximum DC current and frequency interval of interest. Moreover, the effects introduced by such a device can be easily characterized by measurements carried out at its output ports.

The proposed method is here applied to measure the modal complex impedances of an Automotive DC/DC converter in different operation modes. The obtained results allow verifying the existing theory as well as investigating the impact of different operating conditions on the CM and DM impedances. Accuracy of the proposed approach is preliminary verified by measuring the impedance of resistive, inductive and capacitive components. Further measurements carried out by mimicking a noisy environment are presented, aimed at verifying the effectiveness and limitations of the proposed approach in the presence of active components, whose noise current can possibly degrade measurement reliability.

The manuscript is organized as follows. The theoretical study of the CM and DM measurement setups and the mathematical analysis to retrieve modal SMPS complex impedances from measurement data are presented in Section II. In Section III, the proposed measurement procedure is detailed, and possible practical limitations of the method are introduced and discussed. Experimental validation of the proposed approach is presented in Section IV by the use of *ad hoc* set-ups, and validated by measuring the impedance of passive components also the presence of an external noise current. Results of CM and DM impedance measurement for an automotive SMPS under different operating conditions are presented and discussed in Section V. Eventually, concluding remarks are drawn in Section VI.

II. Theoretical Analysis

A. Description and modelling of modal setups

Principle drawings of the modal setups exploited in this work to measure the complex CM and DM impedances (Z_x) of a generic DUT are shown in Fig. 1. The IA is connected to the measurement circuit through a coupling transformer, which provides the galvanic insulation necessary to protect the instrument from the functional voltage and current of the DUT. When measuring the DM impedance is the target (see Fig. 1(a)), the transformer is connected (in series) on one of the two power lines, so that the equivalent impedance seen between the input ports L1 and L2 of the DUT is measured. Conversely, for measuring the CM impedance (see Fig. 1(b)) the transformer can be connected either on a dedicated ground wire (this solution allows the use of the very same transformer both for DM and CM measurement) or, if the ground is not accessible, across the two power lines as a CM choke equipped with a third additional winding used to inject the measuring signal. Eventually, the system is fed through the use of two automotive LISNs [6], providing a stable impedance at the DUT output as well as insulation from the HF noise of the power-supply network.

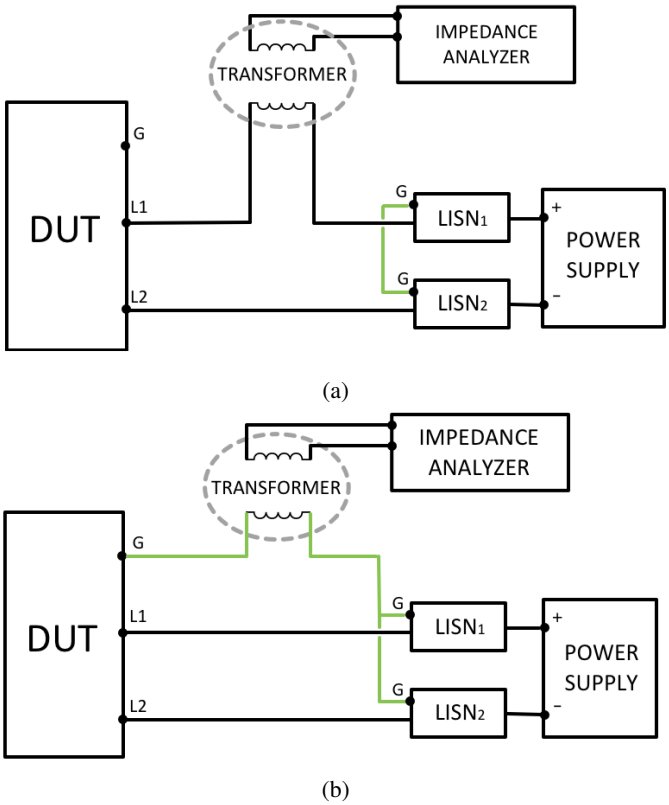

Fig. 1: Principle drawing of the modal measurement circuits: (a) DM, and (b) CM.

An equivalent representation of these setups as seen from the outlets of the IA is shown in Fig. 2. The model of the transformer includes the magnetizing impedance (Z_M), the leakage impedances Z_{LK_1}, Z_{LK_2} of the primary and secondary winding, respectively, and an ideal transformer with transfer ratio n [13]. Inter-winding capacitances are not included, since experimental data proved their negligibility in the frequency range from 10 kHz up to 30 MHz. In passing, it is worth mentioning that the specific transformer model here exploited does not influence the outcome of the impedance extraction procedure. As a matter of fact, a block-box model extracted from measurement data at the transformer ports can be used as an alternative representation, since the procedure only requires the measurement of the short and open-circuit impedances of the transformer. In Fig. 2, the impedances of the two LISNs are gathered into a single component Z^*_{LISN}, which takes different expression, i.e.,

$$Z^*_{LISN} = Z_{LISN_1} + Z_{LISN_2} \tag{1}$$

$$Z^*_{LISN} = \frac{Z_{LISN_1} Z_{LISN_2}}{Z_{LISN_1} + Z_{LISN_2}} \tag{2}$$

for the DM (1) and CM (2) setups in Fig. 1(a) and Fig. 1(b), respectively. Finally, Z_W is associated with the impedance of the test harness. All these aforementioned impedances can be directly measured, so that the only unknown in Fig. 2 is the DUT impedance Z_x.

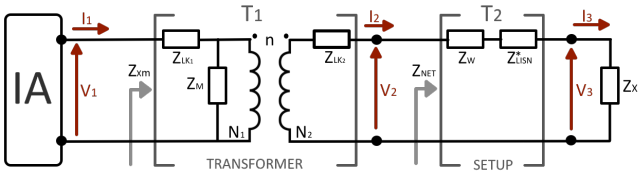

Fig. 2: Circuit representation of the measurement set-up under analysis.

B. Theoretical fundamentals of the proposed method

In order to extract the unknown impedance Z_x from measurement data, two transmission matrices

$$\begin{aligned}\mathbf{T_1} &= \begin{bmatrix} A_1 & B_1 \\ C_1 & D_1 \end{bmatrix} \\ &= \begin{bmatrix} \frac{nZ_{LK_1}+nZ_M}{Z_M} & \frac{n^2 Z_{LK_1} Z_{LK_2}+n^2 Z_{LK_2} Z_M+Z_{LK_1} Z_M}{nZ_M} \\ \frac{n}{Z_M} & \frac{n^2 Z_{LK_2}+Z_M}{nZ_M} \end{bmatrix}\end{aligned} \tag{3}$$

and

$$\begin{aligned}\mathbf{T_2} &= \begin{bmatrix} A_2 & B_2 \\ C_2 & D_2 \end{bmatrix} \\ &= \begin{bmatrix} 1 & Z_W + Z^*_{LISN} \\ 0 & 1 \end{bmatrix}\end{aligned} \tag{4}$$

are associated with the blocks denoted in Fig. 2 as "transformer" and "setup", respectively.

Hence, the relationship between voltages and currents at the IA outlets (port 1 in Fig. 2) and at the DUT input (port 3 in Fig. 2) is expressed as

$$\begin{bmatrix} V_1 \\ I_1 \end{bmatrix} = \mathbf{T} \begin{bmatrix} V_3 \\ I_3 \end{bmatrix} = \begin{bmatrix} A & B \\ C & D \end{bmatrix} \begin{bmatrix} V_3 \\ I_3 \end{bmatrix} \tag{5}$$

where

$$\mathbf{T} = \mathbf{T_1 T_2} \tag{6}$$

with entries

$$\begin{aligned} A =& \frac{nZ_{LK_1} + nZ_M}{Z_M} \\ B =& \frac{n^2 Z_{LK_1} Z_{LK_2} + n^2 Z_{LK_2} Z_M + Z_{LK_1} Z_M + n^2 Z_{LK_1} Z_W}{nZ_M} \\ &+ \frac{n^2 Z_{LK_1} Z^*_{LISN} + n^2 Z_M Z_W + n^2 Z_M Z^*_{LISN}}{nZ_M} \\ C =& \frac{n}{Z_M} \\ D =& \frac{n^2 Z_{LK_2} + Z_M + n^2 Z_W + n^2 Z^*_{LISN}}{nZ_M} \end{aligned} \tag{7}$$

Based on the above expressions, the relationship between the unknown impedance Z_x, i.e.,

$$Z_x = \frac{V_3}{I_3} \tag{8}$$

and the impedance, Z_{xm}, actually measured at the IA ports, i.e.,

$$Z_{xm} = \frac{V_1}{I_1} \tag{9}$$

is retrieved by re-writing (5) as:

$$\frac{V_1}{I_1} = \frac{AV_3 + BI_3}{CV_3 + DI_3} = \frac{A\frac{V_3}{I_3} + B}{C\frac{V_3}{I_3} + D} \tag{10}$$

and by substituting (8). This yields:

$$Z_x = \frac{B - DZ_{xm}}{CZ_{xm} - A} \tag{11}$$

where A, B, C, and D take the expressions in (7).

Although valid for a whatever test setup, actually the application of (11) in practical setups may result to be quite cumbersome. Hence, a wise setup design is here suggested to simplify the proposed procedure, without loss of generality. To this end, a transformer with the same number of primary and secondary windings is considered, which allows the following simplifying assumptions:

$$\begin{aligned} n &= 1 \\ Z_{LK_1} &= Z_{LK_2} = Z_{LK} \end{aligned} \tag{12}$$

By substituting (12) in (11), the unknown impedance Z_x is cast as function of quantities that can be directly measured as:

$$Z_x = Z_o \frac{Z_{setup} + Z_s}{Z_{xm} - Z_o} - Z_{xm} \frac{Z_{setup} + Z_o}{Z_{xm} - Z_o} \tag{13}$$

where: Z_{xm} denotes the impedance that can be actually measured by the IA, $Z_{setup} = Z^*_{LISN} + Z_W$ is the impedance associated with the test setup harness, whereas $Z_o = Z_{LK} + Z_M$, $Z_s = Z_{LK} + Z_{LK}//Z_M$ denote the transformer impedances measured with the secondary winding left open-ended (Z_o) and short-circuited (Z_s), respectively.

III. Proposed Measurement Procedure

For practical implementation of the proposed method, impedances Z_{setup} and Z_x are gathered into a single impedance hereinafter named Z_{NET}. This is done to avoid direct measurement of Z_{setup}, that in some cases is not accessible. Hence, instead of directly measuring Z_{setup}, two indirect measurements are carried out. The former, yielding impedance Z_{NET_1}, involves the set-up impedance (Z_{setup}) and the unknown impedance Z_x. The latter, yielding impedance Z_{NET_2}, involves the series of the set-up impedance (Z_{setup}) and a short circuit instead of Z_x. The impedances Z_{NET_1} and Z_{NET_2} are retrieved from measurement data by means of (11), (3) and (12).

After measuring Z_s, Z_o and Z_{xm}, the unknown impedance Z_x is calculated starting from Z_{NET_1} and Z_{NET_2}, i.e.,

$$Z_{NET_1} = \frac{Z_s - Z_{xm_1}}{Z_{xm_1} - Z_o} Z_o = Z_{setup} + Z_x \tag{14}$$

$$Z_{NET_2} = \frac{Z_s - Z_{xm_2}}{Z_{xm_2} - Z_o} Z_o = Z_{setup} \tag{15}$$

as:

$$Z_x = Z_{NET_1} - Z_{NET_2} \tag{16}$$

Thus, the proposed measurement procedure encompasses the following steps:

1) Calibration of the IA;
2) Connection of the coupling transformer;
3) Measurement of impedance Z_o, with the secondary winding of the transformer left open-ended;
4) Measurement of impedance Z_s, with the secondary winding of the transformer in short circuit;
5) Connection of the test set-up with the IA;
6) Measurement of impedance Z_{xm_1} and calculation of Z_{NET_1} according to (14);
7) Replacement of the unknown impedance Z_x with a short-circuit, measurement of Z_{xm_2} and calculation of Z_{NET_2} according to (15);
8) Evaluation of Z_x as the difference between the aforesaid impedances, (16).

A. Practical limitations of the proposed method

In this sub-section, practical limitations of the proposed method are investigated.

First, since the value of Z_x is retrieved through an indirect measurement, the achievable accuracy strongly depends on the instrument (IA) error, whose uncertainty propagates to (13). From the practical point of view, such an error determines the minimum and maximum impedance magnitude, that can be measured at a specific frequency. These limits (obtained by substituting the unknown impedance with a short-circuit and an open circuit, respectively) are plotted in Fig. 3, and are strictly related to the short-circuit Z_s and open-circuit Z_o impedance of the exploited transformer, respectively. As a matter of fact, if the measurement of Z_s (which is approximately 100 Ω at 10 MHz) is affected by a 1% uncertainty due to limited IA accuracy [12] (here an Impedance Analyzer Keysight E4990A is exploited), it is hard to assure accurate measurement of impedances Z_x (impedance which is in series with Z_s) much smaller than Z_s. In a similar fashion, uncertainty in the measurement of Z_o translates into non-negligible errors in the measurement of impedances Z_x much greater than Z_o. Such a measurement error cannot be completely compensated. Hence, the range of variability of the impedances that can be accurately measured decreases at increasing frequency (see Fig. 3), since Z_s and Z_o respectively increases and decreases. For this reason, the characteristics of the exploited transformer play a role of paramount importance.

Indeed, transformer characteristics might also introduce possible limitations for the DM configuration in Fig. 1(a), since the transformer has to carry the DC functional current of the SMPS without exhibiting saturation (i.e., non linear effects). Eventually, the bandwidth of the transformer shall be suitably selected to match the required frequency range of interest.

In consideration of the aforesaid aspects, the coupling transformer exploited in this work has been specifically designed [14] to withstand the SMPS DC current and to fulfill the desired measurement bandwidth. Characteristics of the adopted

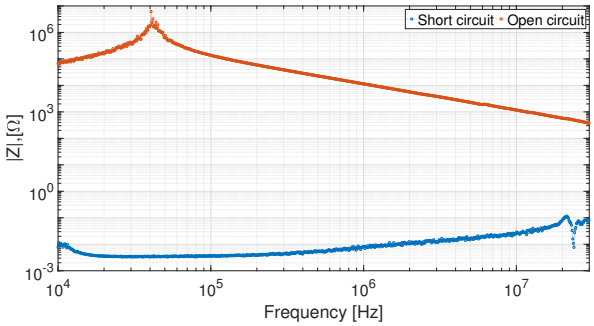

Fig. 3: Minimum and maximum impedance which can be measured by the proposed method.

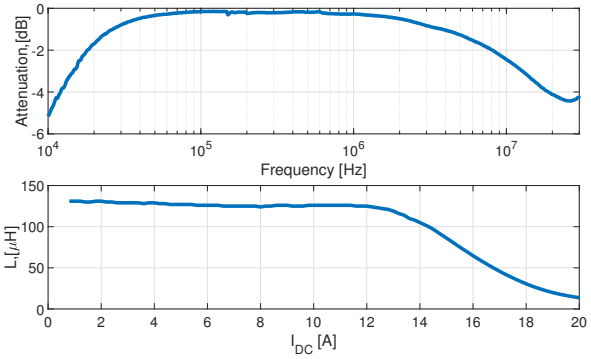

Fig. 4: Transformer bandwidth and saturation curve.

transformer are plotted in Fig. 4. The upper panel shows the transformer frequency response, which is almost flat (with only few dBs of attenuation) in the whole frequency interval of interest. In the bottom panel, the magnetizing inductance is plotted as function of the DC current (saturation curve), thus proving that the adopted transformer can carry a functional DC current up to 13 A without core saturation.

IV. Experimental Validation

A. Validation on passive components

Since the proposed procedure applies both to the CM and the DM setups Fig. 1, for simplicity it will be hereinafter validated by making use of simple (passive) components, whose impedance can be directly measured by the IA and taken as reference quantity. Particularly, the set of passive components exploited for validation includes a resistor $R_{Ref} = 100\Omega$, a capacitor $C_{Ref} = 1\mu$F, and an inductor $L_{Ref} = 88\mu$H, and was selected to cover a wide area of the measurable impedance identified in Fig. 3. For these components, magnitude and phase of the impedance measured by the proposed method are compared versus reference quantities, directly measured at the IA output port, in the plots in Fig. 5. The comparison reveals an appreciable agreement both for the magnitude and phase (with maximum discrepancies on the order of $\pm 5\%$ below 10 MHz). As expected, slight deviation w.r.t. the reference are observed above 10 MHz for those impedances approaching the limit values assigned in Fig. 3. It is worth mentioning that the self resonance peaks, in particular the inductor one,

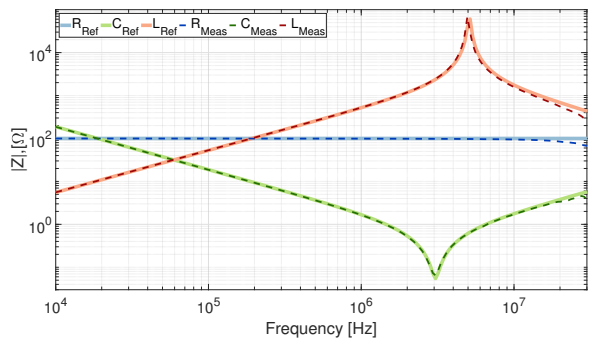

(a)

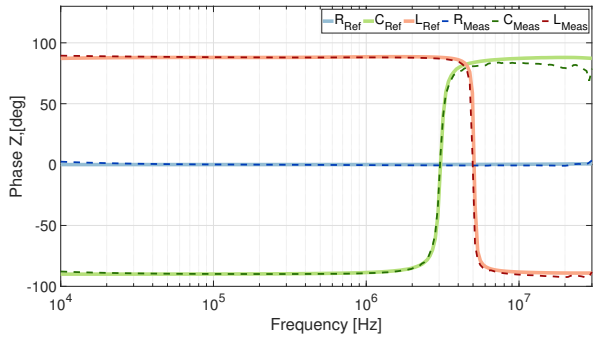

(b)

Fig. 5: Validation on passive components: (a) Magnitude and (b) phase of the impedance measured by the proposed method (dashed curves) vs reference impedance (solid curves).

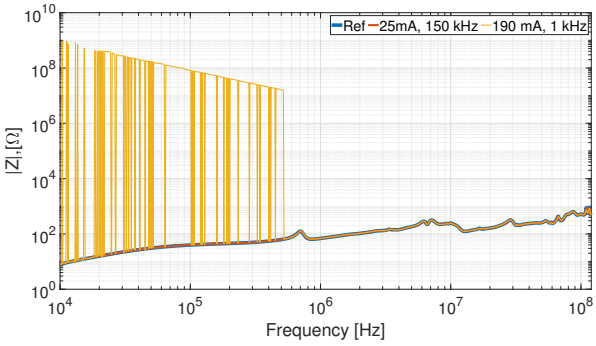

(a)

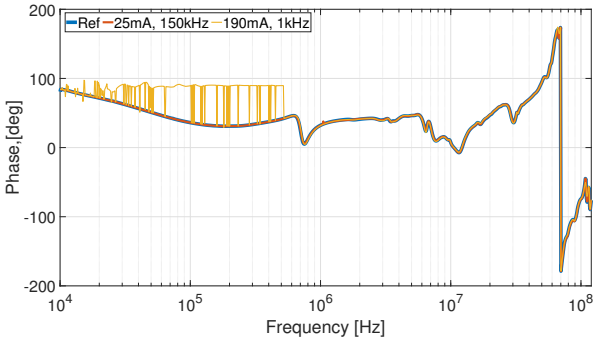

(b)

Fig. 6: Validation of the proposed method in an active system: (a) Magnitude and (b) phase of the impedance measured in the presence of noise currents with amplitude comparable with the IA oscillator current.

exceed the theoretical limits of the measurable impedance. The reason is to be ascribed to the resonance occurring between the transformer itself and the reference impedances, which either decreases (series resonance) the minimum measurable impedance or increases (parallel resonance) the maximum measurable impedance.

B. Validation in an active system

To investigate the ability of the proposed method in correctly measuring the unknown impedance also in an active system, a further experiment is carried out. This is aimed at assessing the robustness of the proposed procedure against the noise (CEs) exiting the converter under standard operating conditions. To this aim, a test bench including the measurement apparatus, an unknown impedance, see the blue trace in Fig. 6, whose value is not relevant for the goal of this validation, and a signal generator was setup. Objective of the test is to experimentally determine the minimum ratio between the IA oscillator current I_{OSC} (maximum value of 20 $\text{mA}_{\text{pk-pk}}$) injected into the system and the maximum noise current of the signal generator I_{noise} assuring reliable measurement. To this end, a controlled noise signal (i.e., a 150 kHz square waveform) was injected into the measurement circuit, and the effect on the measured impedance was observed for increasing amplitude of the injected signal I_{noise}. An example of obtained results is shown in Fig. 6, where the blue curve is measured in the absence of noise and taken as reference. The test revealed that if the amplitude of the injected square wave does not exceeds approximately 25 $\text{mA}_{\text{pk-pk}}$, the measured impedance (red curve) perfectly matches the reference impedance (blue curve). Conversely, for larger noise levels a spurious peak appears in the recorded impedance at the first harmonic frequency (i.e., 150 kHz). The test was then repeated by setting the square-wave fundamental frequency to 1 kHz (so to obtain a continuous spectrum in the frequency interval of interest) and by further increasing the square-wave amplitude (I_{noise}). As an example of the obtained results, one can observe the yellow trace in Fig. 6, where a cluster of spurious peaks can be clearly seen. In this case, the measured impedance exhibits abrupt variations between the reference impedance (blue curve, measured in the absence of noise) and a theoretical curve corresponding to the impedance measured by the IA in the absence of load (1 GΩ at 10 kHz).

In conclusion, for the specific test setup here considered the maximum level of noise which can be stand without degradation of measurement reliability is approximately 25 mA (or 88 dBμA, which is comparable to the highest permitted noise level for CISPR 25 current probe method [5]). In the presence of larger noise levels (i.e., if the ratio I_{noise}/I_{OSC} approximately exceeds 1.25), the IA provides open circuit impedance readings, and the measured impedance exhibits spurious peaks.

To predict in advance this possible limitation, the actual

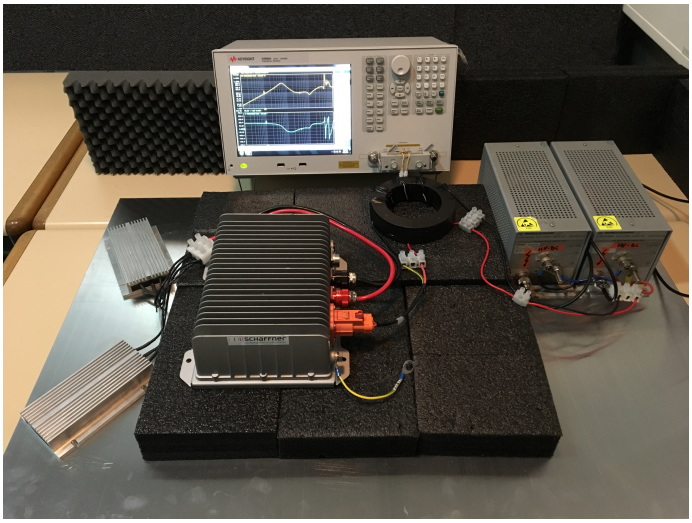

Fig. 7: Experimental test bench compliant with CISPR 25 setup for CE measurement (voltage method).

noise current I_{noise} (i.e., the current in the transformer) can be preliminary measured by adopting the CE setup, current method, foreseen by [5]), and directly compared with the oscillator current I_{OSC} of the IA in use.

Furthermore, this undesired effect can be eliminated by connecting an amplification stage at the IA outlets [12], and by including its effects in the transmission matrix as an additional block. However, it is worth mentioning that this solution was not adopted in this work, since the aforesaid spurious effect was not experienced when measuring the modal impedances of the SMPS under analysis. Indeed, in all experiments the current injected by the IA resulted to be always larger than the noise current exiting the SMPS.

V. Measurement of the SMPS Modal Impedances

The proposed procedure was implemented in a CISPR-25 [5] compliant test set-up for CEs measurement in an automotive environment, with the objective to extract the modal impedances of a DC/DC converter under different operating conditions. The SMPS under investigation is a 2 kW isolated full-bridge DC/DC converter, with input voltage V_{in} = 220V-450 V ($I_{in_{max}}$ = 10 A), output voltage V_{out} = 14 V (I_{out} = 160 A), and switching frequency 80 kHz. A picture of the measurement set-up (DM configuration) is shown in Fig.7. It includes two automotive-compliant [6] LISNs R&S ESH3-Z6 (5μH) and a coupling transformer with a high-permeability nano-crystalline core with four windings both on the primary and secondary side.

A. Measurement of the CM Noise Impedance

The CM impedance was measured from 10 kHz up to 30 MHz in four different operating conditions of the SMPS under test, as shown in Table I.

In addition to the measurements with the SMPS switched off (*Mode 1*) and without load (*Mode 2*), the operating conditions under investigation include: maximum SMPS supply voltage (*Mode 4* and *Mode 5*), minimum SMPS supply voltage (*Mode 2* and *Mode 3*) and high (*Mode 5*) and low (*Mode 3* and *Mode 4*) output current I_{out}. Due to limited capabilities of the DC power supply available for the experiment, the highest secondary current was limited to 63 A *Mode 5*.

TABLE I: SMPS operation modes.

Operation	SMPS	V_{in}	I_{in}	Load	I_{out}
Mode 1	OFF	–	–	–	–
Mode 2	ON	250 V	0.11 A	Open-end	–
Mode 3	ON	250 V	0.4 A	4 Ω	3.5 A
Mode 4	ON	450 V	0.4 A	4 Ω	3.5 A
Mode 5	ON	450 V	2 A	0.22 Ω	63 A

For the measurements, the coupling transformer was connected on a dedicated ground wire between the LISNs and the SMPS. Magnitude and phase of the measured CM impedances are compared in Fig. 8. With the exception of the pronounced resonance observed at 30-50 kHz, all impedances exhibit a capacitive behavior (with estimated capacitance around 1.6nF) up to approximately 1 MHz. Furthermore, it is observed that the impedance measured with the converter off (*Mode 1*, blue curve) is in good agreement with those measured with the converter on. Deviations, due to resonances, are observed beyond 1 MHz, but the trend is the same in all operation conditions, and in spite of the specific load. This suggests the conclusion that the SMPS CM impedance is mainly determined by parasitic (capacitive) couplings between the switching valves and the heat sink [15]–[17] as well as by additional filtering capacitors to ground possibly installed inside the SMPS.

This conclusion is further corroborated by the plots in Fig. 9, where the CEs exiting the SMPS in *Mode 3* and *Mode 4* and measured by a modal CM/DM splitter [18] are plotted along with the corresponding CM impedances. Increasing the supply voltage from 250 V to 450 V significantly increases the measured CEs (with differences up to 15 dB for some spectral lines), while the corresponding CM impedances do not exhibit any appreciable variation.

These results allow concluding that the CM impedance of the SMPS does depend neither on the loading conditions nor on the supply voltage, but it is mainly determined by the specific design of the converter.

B. Measurement of the DM Impedance: Preliminary considerations

With reference to Fig. 10, which schematically represents the impedances involved in the DM test setup (for the SMPS model see [19], [20]), one can infer that correct measurement of the SMPS DM impedance strongly depends on the adopted grounding strategy. As a matter of fact, as long as the SMPS DM impedance is meant as the equivalent impedance seen between L_1 and L_2, the SMPS ground connection becomes of paramount importance to assure reliable measurement. To prove this, the equivalent circuits in Fig. 11 shows the two (DM) impedances measured in the absence, i.e. $Z_{DM_{wo}}$:

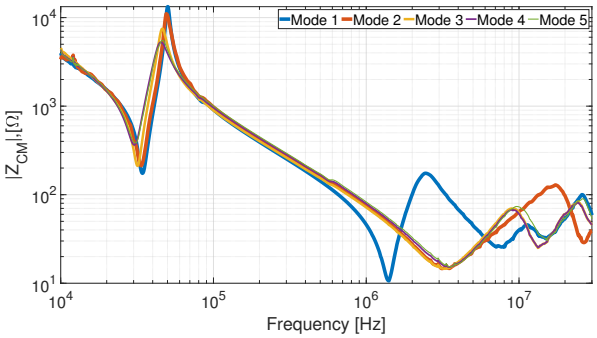

(a)

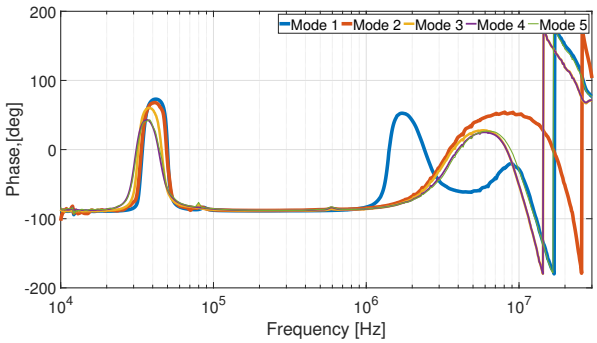

(b)

Fig. 8: CM impedance measured under different SMPS operating modes: (a) Magnitude; and (b) phase.

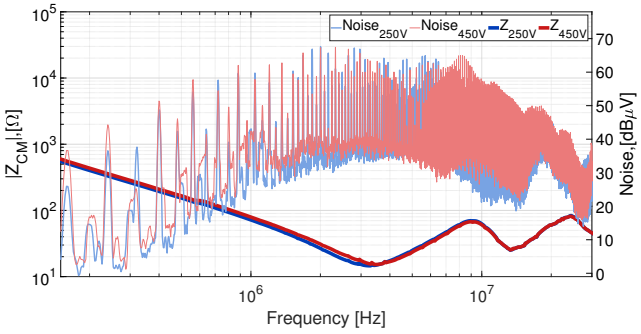

Fig. 9: CM CEs and corresponding impedances measured with 250 V (*Mode 3*) and 450 V (*Mode 4*) supply voltage.

$$Z_{DM_{wo}} = \frac{Z_{LL}(Z_{LG} + Z_{LG})}{Z_{LL} + (Z_{LG} + Z_{LG})}, \tag{17}$$

and in the presence, i.e. Z_{DM_w}:

$$Z_{DM_w} = \frac{Z_{LG}[Z_{LISN} + Z_{LG}Z_{LL}/(Z_{LG} + Z_{LL})]}{Z_{LG} + Z_{LISN} + Z_{LG}Z_{LL}/(Z_{LG} + Z_{LL})} \tag{18}$$

of ground connection between the SMPS and the rest of the measurement setup. Comparison of (17) and (18) suggests the following conclusions. First, the DM impedance measured in the two ground configurations is different. Second, if the SMPS and the rest of the measurement set-up share the same ground, the measured DM impedance Z_{DM} also includes the

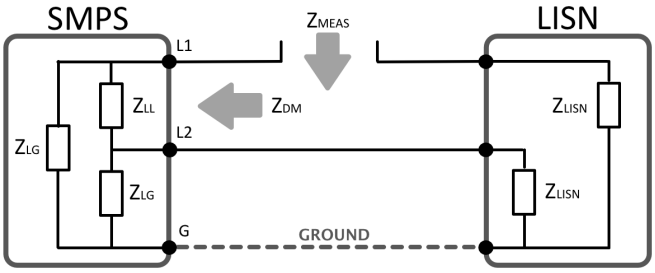

Fig. 10: Equivalent circuit of the DM-impedance measurement set-up as seen from the IA outlets.

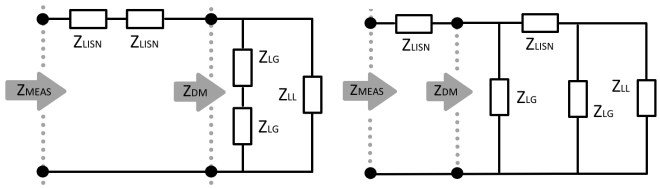

(a) (b)

Fig. 11: Equivalent DM impedance measured (a) without and (b) with grounding of the SMPS.

impedance of the LISN. Based on this preliminary consideration, in the next sub-section, the SMPS DM impedance will be measured without connecting the SMPS to ground.

C. Measurement of the DM Noise Impedance

The measurement of the DM impedance was carried out in the frequency interval from 10 kHz to 30 MHz, by considering the SMPS operating conditions displayed in Table I, with the converter disconnected from ground (according to sub-section V-B).

The measured DM impedances are compared in Fig. 12. Likewise for the CM impedance, when the SMPS is switched off, the DM impedance exhibits a capacitive behavior with magnitude decreasing by a -20dB/dec slope. Since the SMPS under test is not equipped with a DC-link input capacitor, one can infer that the DM impedance measured with the converter switched off is mainly determined by stray capacitances.

The DM impedance measured with the SMPS switched on, see *Mode 2,3,4,5*, is influenced non only by its internal insulation transformer and (possible) output filter [21], that is parameters strictly related to SMPS design, but also by the specific loading conditions [21]. In particular, one can observe the significant difference between the no-load operating condition *Mode 2* and the other modes.

Conversely, the DM impedances measured in *Mode 3-4* and *Mode 5* do not exhibit significant differences, despite the significantly different levels of current at the converter output, that is 3.5 A for *Mode 3-4* and 63 A for *Mode 5*. This scarce sensitivity is in line with the observation that the SMPS DM impedance mainly depends on the load impedance rather than on the output current. Indeed, although the output current changes from 3.5 A (*Mode 3-4*) to 63 A (*Mode 5*), the corresponding load impedance exhibits a negligible variation

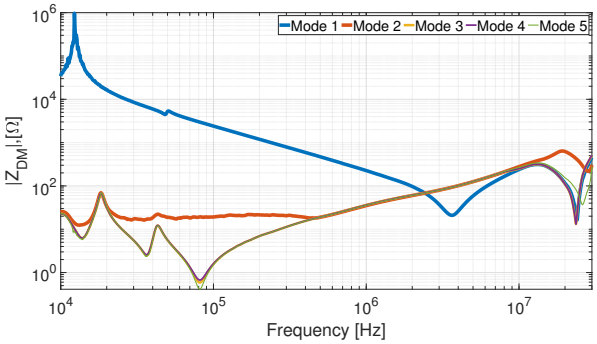

(a)

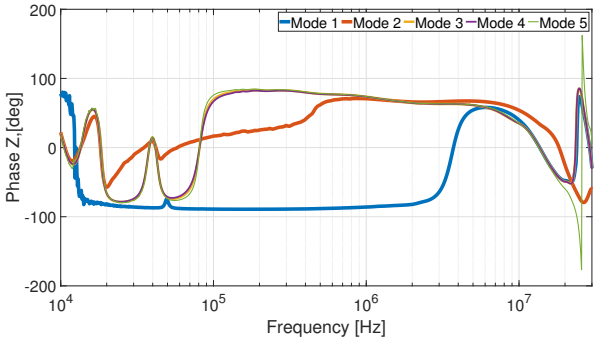

(b)

Fig. 12: DM impedance measured under different SMPS operating modes: (a) Magnitude; and (b) phase.

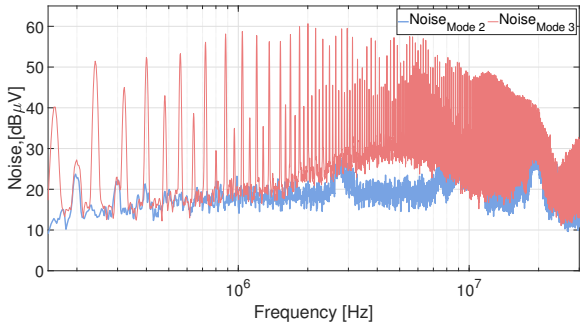

Fig. 13: DM CEs exiting the SMPS under *Mode 2* and *Mode 3* operating conditions.

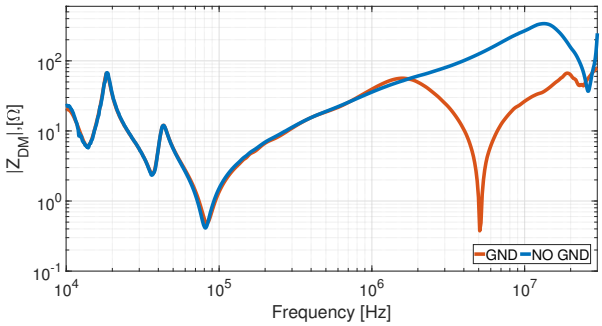

Fig. 14: SMPS DM impedance measured without (blue curve) and with (red curve) ground connection in operation mode 5.

from 4 Ω (*Mode 3-4*) to 0.22 Ω (*Mode 5*). The corresponding CE levels generated by the converter are plotted in Fig. 13, where DM emissions measured in *Mode 2* and *Mode 3* are compared. The observed differences confirm the significant influence that the loading conditions exert on the converter DM emissions.

Moreover, the comparison of the impedances recorded in *Mode 3* (yellow trace in Fig. 12) and *Mode 4* (purple trace in Fig. 12), confirms that the SMPS DM impedance is not influenced by the specific supply voltage.

Eventually, in order to experimentally corroborate the theoretical analysis presented in the previous sub-section, the converter DM impedance (*Mode 5*) was also measured by grounding the SMPS to the same ground of the measurement set-up. The obtained impedance (red curve) is compared versus the one measured without ground connection (blue curve) in Fig. 14. As expected, the comparison outlines differences, which become significant especially beyond 1 MHz.

VI. Conclusion

In this work, a novel measurement method has been presented, which is aimed at characterizing not only the magnitude but also the phase of the CM and DM impedances of a SMPS under different working conditions. The procedure was preliminary validated by measuring the impedance of passive components. Moreover, to assess feasibility of the proposed procedure also in active systems, an *ad hoc* conceived experiment was carried out, which involves an additional signal generator to mimick the noise exiting the SMPS. Eventually, the modal impedances of an automotive SMPS were measured under different operating conditions in a CISPR 25 compliant test set-up.

It was observed that the CM impedance does not depend on the specific operating condition of the SMPS, being just influenced by parasitic capacitive coupling with the heat sink as well as possible capacitive filters installed inside the converter. As far as measurement of the DM impedance is concerned, it was proven that it should be measured with the SMPS floating with respect to ground. Furthermore, a significant sensitivity to the specific operating conditions (i.e., converter on/off and presence/absence of the load) was observed.

These results can be conveniently exploited in designing active and passive EMI filters since information not only on the magnitude but also on the phase of the SMPS under analysis are key ingredients to achieve an effective filter design (e.g., to select the most suitable filter configuration). In this regard, a common best practice is to consider CM and DM impedances of SMPSs respectively much higher and much smaller than the network impedance. However, the results presented in Fig. 8 and Fig. 12 show that such a simplifying assumption is not always strictly verified in the whole frequency interval for CE measurement.

REFERENCES

[1] M. L. Heldwein, H. Ertl, J. Biela, and J. W. Kolar, "Implementation of a transformerless common-mode active filter for offline converter systems," *IEEE Trans. Ind. Electron.*, vol. 57, no. 5, pp. 1772–1786, May 2010.

[2] A. Amaducci, "Design of a wide bandwidth active filter for common mode emi suppression in automotive systems," in *Proc. IEEE Int. Symp. Electromag. Compat. & Signal/Power Integrity (EMCSI)*, Aug 2017, pp. 612–618.

[3] R. Goswami and S. Wang, "Modeling and stability analysis of active differential-mode emi filters for ac/dc power converters," *IEEE Trans. Power Electron.*, vol. 33, no. 12, pp. 10 277–10 291, Dec 2018.

[4] K. Li, K. See, and F. Fan, "Study of emi filter performance without lisn based on noise impedances," in *Proc. Asia-Pacific Int. Symp. Electromag. Compat. (APEMC)*, June 2017, pp. 115–117.

[5] *CISPR 25 - Vehicles, boats and internal combustion engines Radio disturbance characteristics Limits and methods of measurement for the protection of on-board receivers*, 2016-10.

[6] *CISPR 16 - Specification for radio disturbance and immunity measuring apparatus and methods Part 1-2: Radio disturbance and immunity measuring apparatus Coupling devices for conducted disturbance measurements*, 2011-06.

[7] D. Y. Chen, M. J. Nave, and D. Sable, "Measurement of noise source impedance of off-line converters," *IEEE Trans. Power Electron.*, vol. 15, no. 5, pp. 820–825, Sep. 2000.

[8] V. Tarateeraseth, B. Hu, K. Y. See, and F. G. Canavero, "Accurate extraction of noise source impedance of an smps under operating conditions," *IEEE Trans. Power Electron.*, vol. 25, no. 1, pp. 111–117, Jan 2010.

[9] K. Y. See and J. Deng, "Measurement of noise source impedance of smps using a two probes approach," *IEEE Trans. Power Electron.*, vol. 19, no. 3, pp. 862–868, May 2004.

[10] X. Shang, D. Su, H. Xu, and Z. Peng, "A noise source impedance extraction method for operating smps using modified lisn and simplified calibration procedure," *IEEE Trans. Power Electron.*, vol. 32, no. 6, pp. 4132–4139, June 2017.

[11] F. Zheng, W. Wang, X. Zhao, M. Cui, Q. Zhang, and G. He, "Identifying electromagnetic noise-source impedance using hybrid of measurement and calculation method," *IEEE Trans. Power Electron.*, vol. 34, no. 10, pp. 9609–9618, Oct 2019.

[12] K. Technologies, *Impedance Measurement Handbook*, 2016. [Online]. Available: https://literature.cdn.keysight.com/litweb/pdf/5950-3000.pdf

[13] J. Biernacki and D. Czarkowski, "High frequency transformer modeling," in *Proc. IEEE Int. Symp. Circuits and Systems*, vol. 3, May 2001, pp. 676–679.

[14] N. Kondrath and M. K. Kazimierczuk, "Bandwidth of current transformer," *IEEE Trans. Instrum. Meas.*, vol. 58, no. 6, pp. 2008–2016, June 2008.

[15] I. A. Makda and M. Nymand, "Common mode noise generation and filter design for a hard switched isolated full-bridge forward converter," in *Proc. 40th Annual Conf. IEEE Ind. Electron. Society*, Oct 2014, pp. 1312–1317.

[16] T. Q. Zheng, "Common mode noise modeling and analysis of full-bridge dc-dc converter," in *Intelec 2012*, Sep. 2012, pp. 1–7.

[17] H. Chen, L. Feng, W. Chen, and Z. Qian, "Modeling and measurement of the impedance of common mode noise source of switching converters," in *Proc. IEEE Applied Power Electron. Conf. and Exposition*, March 2006, p. 4.

[18] K. Y. See, "Network for conducted emi diagnosis," *Electronic Letters*, vol. 35, no. 17, pp. 1446–1447, May 1999.

[19] M. Foissac, J. Schanen, and C. Vollaire, "black box emc model for power electronics converter," in *Proc. IEEE Energy Conversion Congress and Exposition*, Sep. 2009, pp. 3609–3615.

[20] M. Jin, M. Weiming, and Z. Lei, "Determination of noise source and impedance for conducted emi prediction of power converters by lumped circuit models," in *Proc. IEEE 35th Annual Power Electronics Specialists Conference*, vol. 4, June 2004, pp. 3028–3033.

[21] I. A. Makda and M. Nymand, "Differential mode emi filter design for isolated dc-dc boost converter," in *Proc. Conf. Power Electron. and Applications*, Aug 2014, pp. 1–8.

Enrico Mazzola was born in Lecco, Italy, in 1992. He achieved the double M.S. degree in Electrical Engineering at Politecnico di Milano, Milan, Italy, and at Xi'an Jiaotong Univesity, Xi'an, China, in July 2017. In September 2017 he joined the automotive R&D division of Schaffner Group in Luterbach, Switzerland, as an executive Ph.D. student in Electrical Engineering with Politecnico di Milano.

His main research interests in the field of EMC and power electronics include active and passive EMI filtering techniques for automotive applications, the study of magnetic materials and measurement techniques.

Flavia Grassi (M'07−SM'13) received the Laurea (M.Sc.) and Ph.D. degrees in electrical engineering from Politecnico di Milano, Milan, Italy, in 2002 and 2006, respectively.

She is currently an Associate Professor with the Department of Electronics, Information and Bioengineering, Politecnico di Milano. From 2008 to 2009, she was with the European Space Agency, The Netherlands, as a Research Fellow. Her research interests include distributed parameter circuit modeling, statistical techniques, characterization of measurement setups for EMC testing, and powerline communications.

Dr. Grassi was the recipient of the URSI Young Scientist Award, in 2008, and the IEEE Young Scientist Award at the 2016 Asia-Pacific Int. Symp. on EMC (APEMC). She was also the recipient of the IEEE EMC Society 2016 Transactions Prize Paper Award and the Best Symposium Paper Award from the 2015 APEMC and from the 2018 Joint IEEE EMC & APEMC Symposium.

Alessandro Amaducci was born in Forlí, Italy, in 1988. In 2015 he received his M.S. degree with honors in Electrical Engineering from Politecnico di Milano, Milan, Italy. Nowadays he leads the Automotive R&D team of Schaffner Group where he is carrying on his development on Active and Passive EMI filtering integration in Automotive Systems.

He is the author of several patents on EMI filtering and his research interests include power conversion, electromagnetism, magnetic materials, active EMI filtering and design for manufacturing according to Automotive standards.